POROUS SILICA PLATFORMS (PSP) FOR CARBON CAPTURE TO MITIGATE CLIMATE CHANGE

By

Nicholas Pizzi

A THESIS

Submitted to the faculty of Delaware State University
in partial fulfillment of the requirements
for the degree of Master of Science in the
Department of Chemistry

DOVER, DELAWARE

August 2017

This thesis is approved by the following members of the Final Oral Review Committee:
Dr. Chen-Yu Lai, Committee chairperson, Department of Chemistry, Delaware State University
Dr. Andrew Goudy, Committee Member, Department of Chemistry, Delaware State University
Gabriel Gwanmesia, Committee Member, Department of Physics, Delaware State University
Gulnihal Ozbay, Committee Member, Department of Agriculture, Delaware State University

ACKNOWLEDGMENTS

To Dr. Chen-yu Lai and Dr. Daniela Radu, thank you for taking a chance on a veteran with an online psychology degree. I have learned more in the past two years under your tutelage than I have in all the other years of my life combined.

To my classmates for the study sessions, help, and allowing me the chance to help them.

To Jessica Brown for always telling me what I needed to hear, even if I didn't want to hear it

To Nicole Horn for reminding me to always read the manuals.

To Sage Kekoa for teaching me, "the hammer of knowledge is nothing without the wisdom of aim."

Finally, I would like to thank my committee members, Drs. Andrew Goudy, Gabriel Gwanmesia and Gulnihal Ozbay for their valuable suggestions and comments on my thesis research.

I would like to thank The Department of Energy, for funding me and my project.

POROUS SILICA PLATFORMS (PSP) FOR CARBON CAPTURE TO MITIGATE CLIMATE CHANGE

Nicholas Pizzi

Faculty Advisor: Dr. Cheng-yu Lai

ABSTRACT

My research objective is to find an improved functionalized solid silica support for Carbon dioxide (CO_2) to mitigate climate change, by finding an optimal silica nanoparticle morphology and amine capture system. Climate change threatens the continued existence of Earth as a habitable planet for humans. The causes for climate change are varied, but the most alarming are the anthropogenic factors, chiefly greenhouse gasses. Carbon dioxide (CO_2) is one of the main components of greenhouse gasses, and in lieu of non-polluting energy sources, efforts must be made to limit the amount of CO_2 we contribute. One strategy is post-combustion capture of CO_2, using amines. The use of liquid amine solutions is not feasible due to the additional burden placed on equipment exposed to amines. Furthermore, the reduction in CO_2 at a power plant is offset by the increased amount of raw materials needed to meet energy demands due to the reduced production efficiency when using liquid amines. Solid support for amines is an attractive option to mitigate the pitfalls realized when using amines for post combustion capture. Of the different types of materials (zeolites, Metal Organic Frameworks—MOFs, and nanoparticles and other, not otherwise specified nanomaterials), silica nanoparticles have been shown to be the best option yet due to tunable pore sizes, pore morphologies, and high surface area to weight ratios. In my work, using a well-known silica nanoparticle synthesis, I was able to

direct a stellate shaped particle (hierarchical pore structure) to achieve a remarkable 4.6 mmol/g of CO_2 capture using Tetraethylenepentamine (TEPA) as the amine.

Table of Contents

LIST OF TABLES

LIST OF FIGURES

LIST OF ABBREVIATIONS

BET	Brunauer-Emmett-Teller
CTAB	Cetrimonium Bromide
CTATos	Cetyltrimethylammonium tosylate
FT-IR	Fourier-Transform Infrared (spectroscopy)
MSN	Mesoporous Silica Nanomaterial (Nanosphere)
SEM	Scanning Electron Microscope
TEPA	Tetraethylenepentamine
TEA	Triethanolamine
TEM	Transmission Electron Microscope
TEOS	Tetraethyl orthosilicate

CHAPTER 1. INTRODUCTION

1.1 Background

Since the 1960's, climatological studies suggested the possibility for overall global warming due to anthropogenic causes, chiefly the use of fossil fuels, in which combustion results in several gasses that have the ability to trap radiative energy and warm the earth. Computer models using known data showed this to be true. Since, then the models have shown to be wrong; they predicted a slower warming effect, with more immediate results. However, we have measured faster warming, yet the results of which were far more complicated. While the disastrous effects have not come to full realization, other effects not predicted have manifested, developing a clearer picture of how climate change will affect us. These confounding variables along with contrarian data collected using inaccurate experimental design and analyzed using non-standard algorithms have been used by some to claim climate change is in error.

Dr. Roy Spencer is a former NASA climatologist who presents such data (**Figure 1**). According to him, the overall warming since 1979 is only 0.27°C (this is only a relativistic measurement representing the departure from 0°C, and does not take into account actual difference between his data from 1979 to 2017, which is (by using the same metric) is less than 0.72°C of NASA's measurement (0.99°C) and an overwhelming consensus of other independent, international organizations (**Figure 2**). NASA and other global agencies, utilize temperature measurements taken from the surface (land and water), and average these over time. Dr. Spender maintains lower tropospheric measurements (LTM's) for more accurate outcomes. From a

thermodynamics perspective, it would make more sense to use below LTM plot and NASA figure.

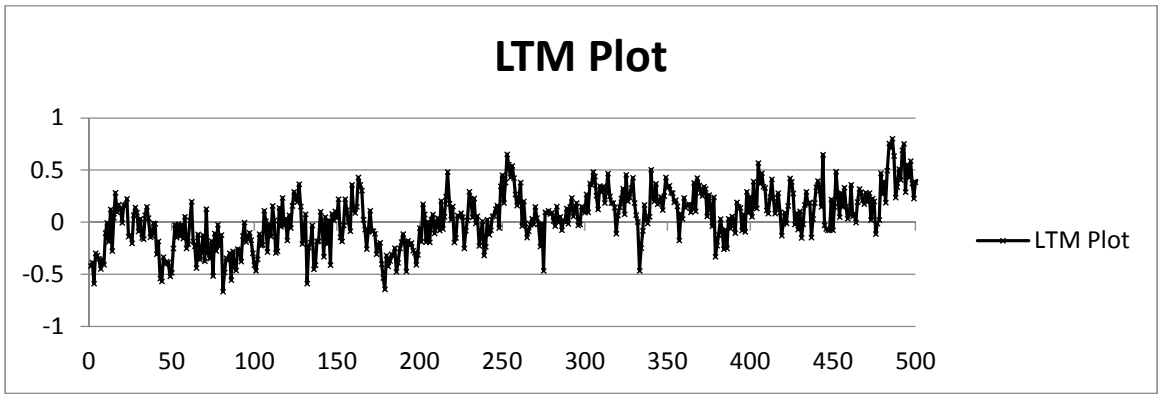

Figure 1. Lower Tropospheric Measurements show little warming when presented as monthly averages with a 13 month running average (produced by Dr. Roy Spencer).

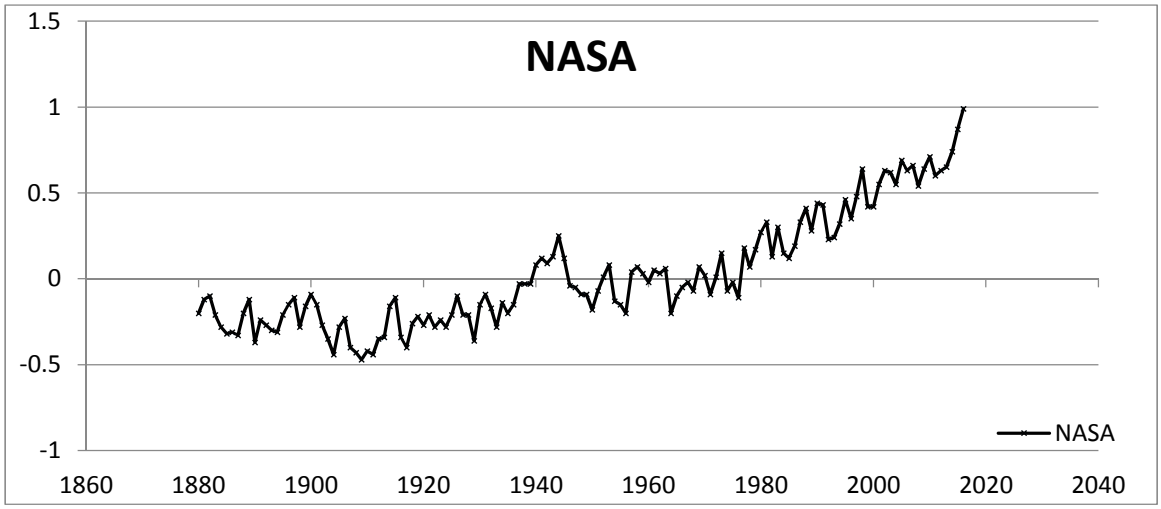

Figure 2. Data collected by NASA shows a warming trend.

Temperatures collected from the surface, as the solid and liquid states of matter (land and water) would represent a more stable measurement of total input of heat than the atmosphere. Also, Dr. Spencer's LTM's measurement for luminosity is based on atmospheric oxygen.

Considering the cause for climate change is the result of greenhouse gasses (CO_2), and then it is likely any heat being trapped, is contained by a thermocline defined by a maximum energy level of CO_2. This thermocline is at a lower altitude than the LTM's thus any atmospheric oxygen being measured will reflect a lower temperature.

While this explains a discrepancy between the measurements in terms of magnitude, it does not explain the overall difference in trends. When comparing both data sets the following metrics are apparent: i) both list global average temperatures taken from multiple places and ii) both list global average temperatures taken at regular time intervals, and both use a running average. However, NASA averages yearly temperatures, and uses a 5-year running average, while Dr. Spencer uses monthly average temperatures and uses a 13-month running average. Also, NASA lists data points from as early as the 1880's while Dr. Spencer begins his data set from 1979. Finally, both lists have different statistical methods to validate their data.

An in-depth analysis of statistical methods is beyond the scope of this paper. However, a simple normalizing of the data sets is possible. To do this, the raw data from each set was extracted. Since NASA lists only yearly average yearly temperatures, Dr. Spencer's monthly averages were used to produce the yearly averages (this is statistically sound assuming both data sets are produced initially from independent and routine measurements). Next, all data from prior to 1979 was removed from the analysis. Finally, the running averages were removed from consideration and a linear regression was used to show general trend with respect to time (positive, negative, or neutral). When plotted against each other, both graphs initially show a

similar pattern of highs and lows (the absolute difference between time equivalent points was measured and analyzed $\mu = 0.4339$ $\sigma = 0.0995$) (**Figure 3**).

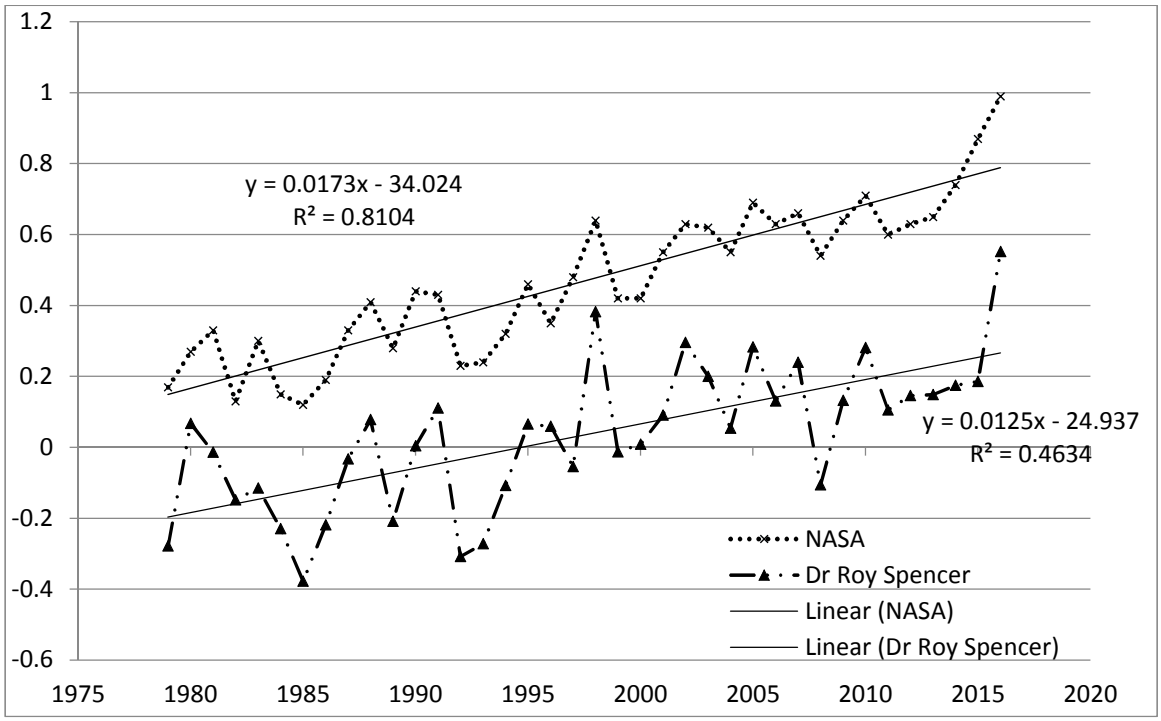

Figure 3. When the two data sets are displayed using the same parameters, they show a similar pattern. Both data sets agree, the overall trend is that of warming.

The linear regression for both lines both show a positive correlation though Dr. Spencer's shows a smaller rate of change (NASA = 0.017 Spencer = 0.013) and a smaller r^2 (NASA = 0.81 Spencer = 0.46). The difference in rate of change and r^2 values can most likely be attributed to the issues with measuring atmosphere as explained above (less stable measurement, medium is less affected due to thermocline). Furthermore, both data sets were compared against each other form relative normative distribution and showed similar characteristics about the mean, albeit

with a difference of means (NASA: $\mu = 0.469$ $\sigma = 0.21$/ Spencer: $\mu = 0.038$ $\sigma = 0.20$), (**Figure 4**). This further demonstrates that one of sited contrarian scientists used to debunk climate change literature actually agrees with the assertion presented by other global agencies that Earth over all is warming. By zeroing the linear regressions so that they originate from a common origin (0,0), and extending into the future, it is clear that when using Dr. Spencer's data, we will reach NASA's current average global temperature by 2030 +12 years (**Figure 5).** While Dr. Spencer is only one of several scientists with oppositional data, similar transparent methods should be used as a means of comparison.

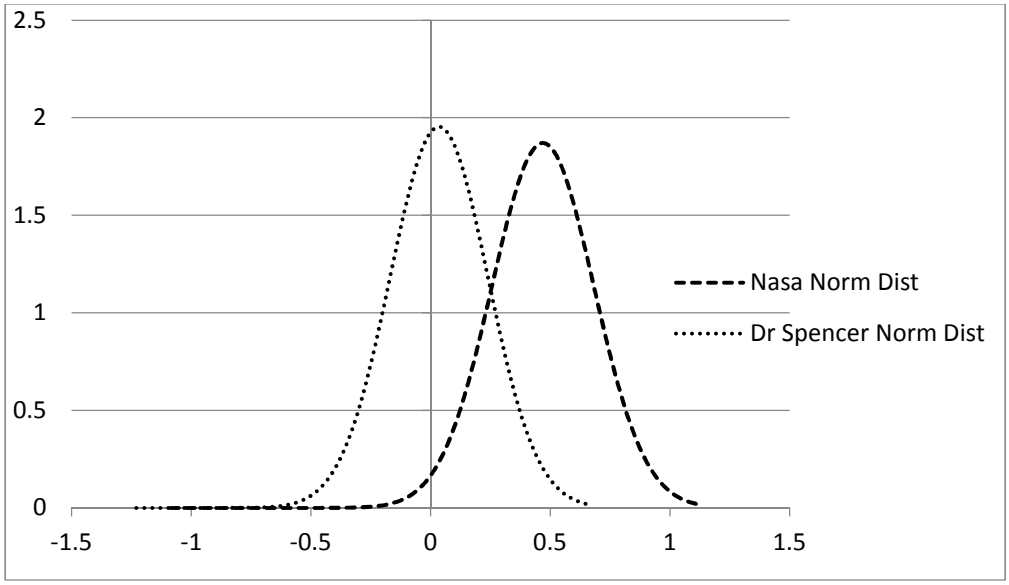

Figure 4. Normal distributions of the two data sets. Both show similar characteristics, yet suggest different populations, corresponding to the two different methods of measuring.

Several factors are attributed to the overall warming. Of primary concern, is the dependence on fossil fuels, and manufacturing processes resulting in release of "greenhouse gasses?" Here we focus on one of the greenhouse gasses, CO_2.

Ideally, the move from fossil fuels in favor of clean energy would eliminate the continued emission of CO_2.

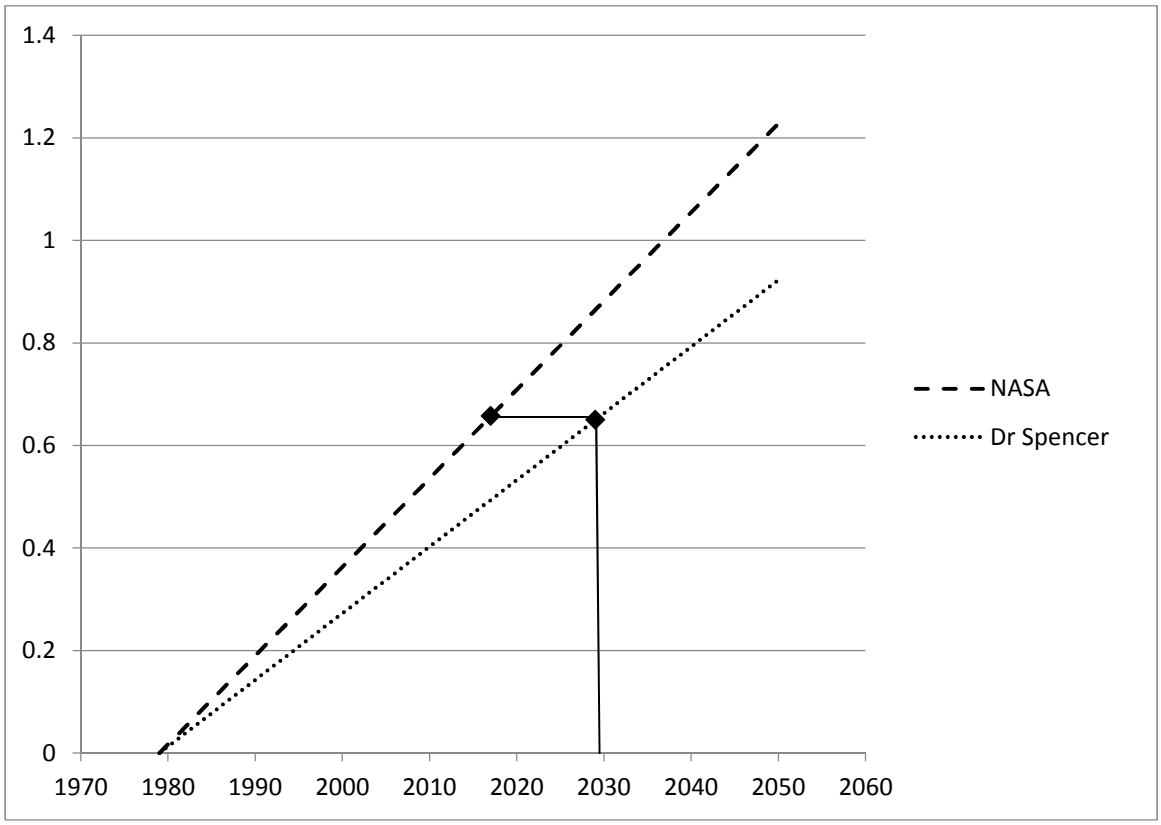

Figure 5. When the linear regressions are plotted together as a function of time and zeroed to show magnitude of change, contrarian data shows the current accepted temperature offset by only 12 years (2029).

In the meantime, the mitigation of CO_2 must be considered. CO_2 may be sequestered prior to fossil fuel combustion (removing CO_2 prior to combustion), reducing the amount of CO_2 during combustion via oxy-combustion, or catching and sequestering CO_2 post combustion. The post-combustion process is attractive since unlike pre and oxy combustion does not require additional steps in processing or expensive chemical looping. The process is simple as CO_2 will readily bond to amine functional groups forming carbamate salts. However, despite the

attractiveness of post-combustion sequestration, the use of liquid amines poses several obstacles. Liquid amines corrode equipment, resulting in a shorter lifespan, and thus increased cost. In addition, liquid amine compounds bond CO_2; they become viscous, lowering the efficiency of equipment. This result in an increase need of raw material, thus any reduction in CO_2 during combustion, is offset by the additional CO_2 released during increased burning when supplying the increased need of raw materials. A solid support for amines would prevent these obstacles.

Since they were first theorized, nanoparticles have been thought to open new avenues in the fields of manufacturing, material chemistry, catalytic chemistry, and bio-medical applications. Different classes of nanoparticles and nanostructures exist. Research has been done using zeolites, metal organic frame works, and the wide variety of nanoparticles that do not fit within the description of the former two. Despite the varying synthesis and associated methods of control to tune physical characteristics of nanoparticles for many elements, Silicon is of interest due to its relative abundance, ease of synthesis, bio-compatibility, relative non-toxicity to the environment, and as was later demonstrated by many research teams, reaction directed morphology and tunable pore sizes. Furthermore, due to the chemical nature of the silica nanoparticles, their surfaces are easily functionalized adding to their versatility in a wide range of applications. Furthermore, within the context of CO_2 capture, silicon nanoparticles show higher or equal capture efficiency as zeolites and MOF's. I was able to capture 4.6 mmol of CO_2 per gram of amine functionalized silica nanoparticle. One of the highest capture efficiencies listed for zeolites (ZIF-69) is 83 liters of CO_2 per liter of zeolite. Comparing these two by converting mmol/g shows our nanoparticles are able to achieve 268.8 liters of CO_2 per liter.

Similarly for MOF's, Mg-MOF-74 shows one of the highest capture efficiencies at 27.5% weight percentage. Again, comparing this by converting mmol/g shows our particles are achieving 26% weight percentage capture efficiency. While this is slightly less than the MOF, silicon is far more cost effective than a solid support using metals. Considering the relative costs of metals and silicon, it is clear silica nanoparticles are currently the best choice as a solid support platform for post combustion CO_2 capture.

Stöber (1968) first demonstrated the synthesis of silica nanoparticles in 1968. The Stöber process is a wet chemical approach to silica nanoparticle synthesis and demonstrates the use of the sol-gel process. The synthesis is a two-step mechanism: hydrolysis and co-condensation. A silica precursor ($Si(OR)_4$) is reacted in a water-alcohol solution, where the precursor is hydrolyzed producing SiOH and alcohols. The Silanols then further react with either available water or alcohols in during the co-condensation pathway producing SiO_2 polymers, water and alcohols. The resulting nanoparticle's size is monodispersed, solid spheres. Altering reaction conditions (concentrations of reactants), yields varying monodispersed nanoparticles. The addition of surfactants past the micelle critical concentration, provides a template for SiO_2 to condense around, producing varying morphologies of mesoporous silica nanoparticles (e.g. uniform cylindrical, worm-like, stellate). The ability to control size, morphology and pore characteristics lend to the interest different fields have in silica nanoparticles. Of interest to us is

their ability to scrub carbon dioxide from manufacturing processes and energy production, and the potential as non-viral vectors for targeted drug and gene therapy.

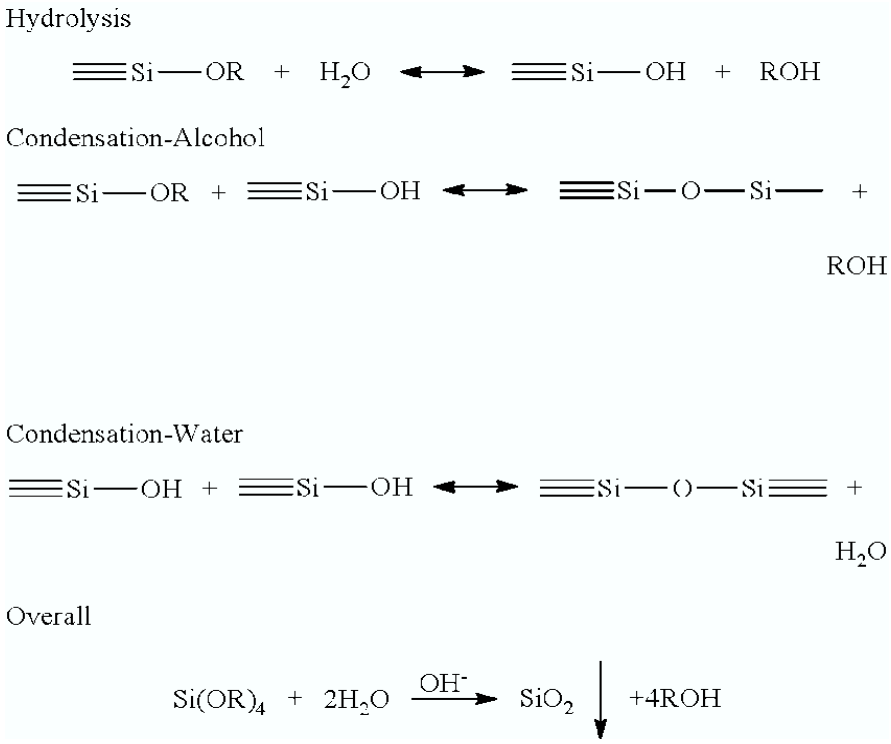

Equation 1. Stöber mechanism.

Due to rising global temperatures as a result of anthropogenic factors, a way to reduce "greenhouse" gasses (e.g. NO, SO_2, CO_2) is vital. While alternative green energy is a rapidly expanding field, several factors prevent it from being an immediately viable solution to greenhouse gas emissions by lessening our dependence on fossil fuels. Another approach is to

mitigate the effects of the human impact on the environment, is to capture and sequester greenhouse gasses at the source. Specifically, CO_2 can be captured during one of three phases: post-combustive, pre-combustive, or oxy-combustive. While all three methods may be facilitated by the use of nanoparticles, pre-combustive and oxy-combustive require chemical looping, which is prohibitive in cost and efficiency. Post-combustion avoids the need for chemical looping, but has its own pitfalls. The use of liquid amines to capture CO_2 has been well known but presents several problems. Liquid amines corrode equipment resulting in increased maintenance and replacement costs. The carbamates (secondary amine-CO_2 terminal product) and hydrogen carbonates (tertiary amine-CO_2 terminal product) oxidize and thus degrade the unreacted amines, lowering the overall efficiency of CO_2 capture. Furthermore, flow problems arise as a result of increased viscosity as liquid amines and CO_2 react. These problems result in an increase in consumption of fuel, and overall less efficient processes. Any reduction in CO_2 emissions at the manufacturing process/energy production are offset by the added CO_2 emissions during the extraction and transport of fossil fuels due to the increased amount of fossil fuels needed to meet the efficiency gap caused by the use of liquid amines. A solid support would mitigate or eliminate these obstacles.

Solid silica nanomaterials offer a viable platform for which to attach amine functional groups. The first generation of SNP's researched was Mesoporous Silica Nanosheets (MSN's). These materials exhibit a high surface (>1000m^2/g) areas and pore volumes (> 1ml/g). However due to the pore morphology, (relatively narrow, long, cylinders, <4nm), functionalization, and subsequent carbon capture was hindered by close-packed amines at the pore entry, resulting in a

loss of usable inner pore space. While this is an improvement over other nanomaterials (e.g. zeolites, metal organic frameworks, and carbon nanotubes) it does not make up for the overall loss. The ability to control both size and porosity characteristics allow for a hierarchical pore structures (small shallow pores within larger pores). While this morphology exhibits less total surface area and pore volumes than the previous MSN's they show higher loading and capture potential due to the more easily accessed internal surface area.

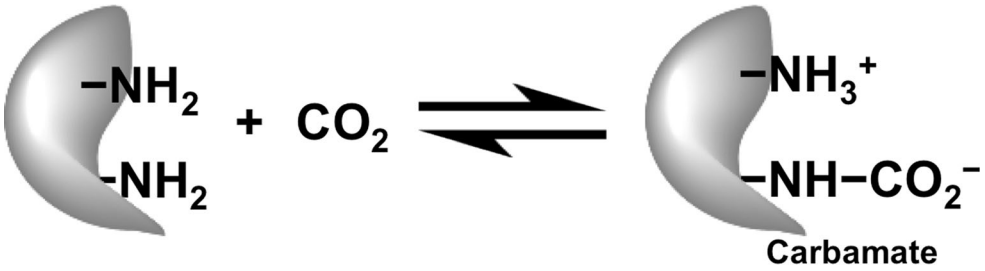

Figure 6. Chemistry of CO_2 capture through reaction with solid-supported amines on porous supports located in close proximity (schematic of porous scaffold pore section).

In addition to SNP morphology, selection of the functional amine is an important factor to optimize CO_2 uptake. Tetraethylenepentamine (TEPA) offers a stable amine compound able to accept multiple CO_2 molecules. One trade off of employing a larger molecule however is packing efficiency and pore blocking.

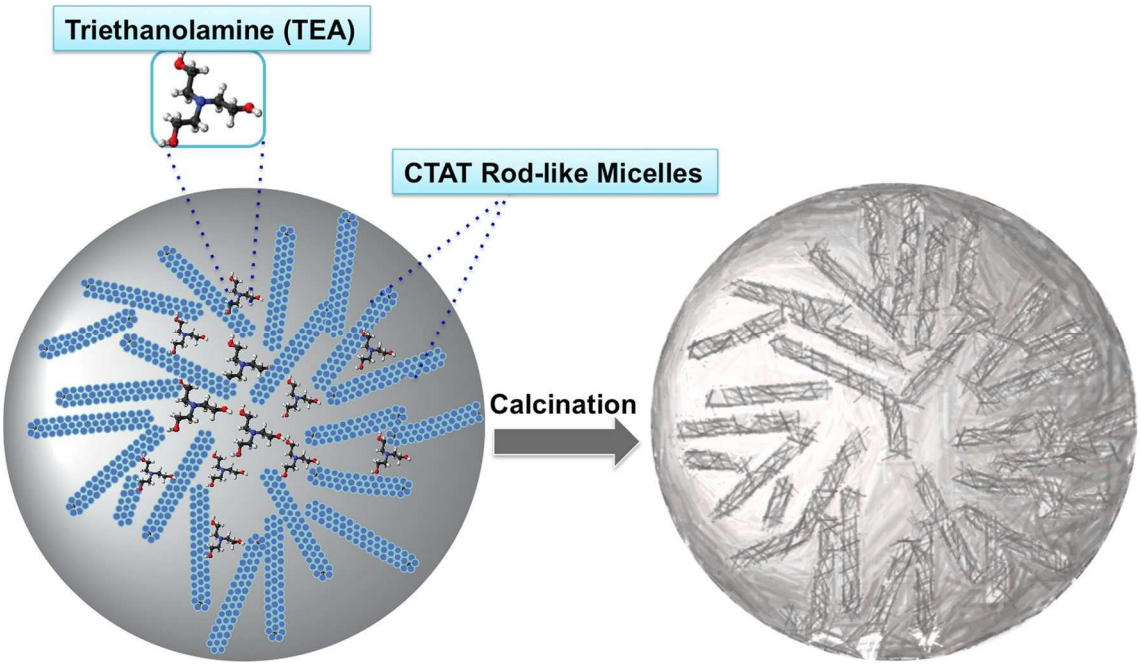

Figure 7. Schematic representation of stellate MSN formation.

Using TEPA on a stellate nanoparticle we were able to obtain an adsorption efficiency of 4.6 mmol/g. The theoretical adsorption for an equal volume of the liquid amine is 9.2 mmol/g. The efficiency loss is attributed to pore packing and blocking as increased amine is loaded. We attempted to resolve this using a pore swelling agent to create Mesoporous Organosillica Nanoparticles (MONs). Unfortunately, the MONs did not offer enough attachment sites for the amine and showed no improvement. It is clear from our study the optimization of particle size, pore morphology, and functional amine is the key to making further improvements.

CHAPTER 2. LITERATURE REVIEW

2.1. Methodology and Results of Calculating Central California Surface Temperature Trends: Evidence of Human-Induced Climate Change

To support global climate change which is based on average temperatures, a detailed look at a small regional area was critically analyzed in California. More specifically, this analysis tested a supporting hypothesis that century-scale trend differences should be identifiable between irrigated and non-irrigated regions. Central California stations were examined, with attention on discontinuities in data collection. This method highlights homogenous segments of data. Biases are then determined at each segment and controlled for between segments. This rigorous mathematical modeling allows the segments to be merged and completing a complete regional time series. Maximum and minimum temperatures were completed from multiple stations in an irrigated area while several stations in a nearby non-irrigated area were considered for the time period covering 1910-2003. This modeling supports the differences hypothesis. This analysis shows a difference in warming rates between irrigated and non-irrigated areas (irrigated areas having a faster rate).

2.2. Assessing Agricultural Risks of Climate Change in the 21st Century in a Global Gridded Crop Model Intercomparison

Global Gridded Crop Models (GGCMs) are used to determine the effects expected based on average global climate models. These models are an important tool to plan for future crop shortfalls if climate change isn't slowed. Seven models, grouped into three types (site-based crop models, agro-ecosystem models, and agro-ecological zone models), differ in several ways

depending on the type of model: inclusion and parameterization of soil and crop processes, management inputs and outputs. The comparison of results is similar between models except for mid-latitude regions. Modeling in this area shows uncertainty, and highlights a need for further research to determine the effects of increased atmospheric CO_2. However, despite the uncertainty at mid-latitude regions, the models are fairly consistent and in agreement at high and low latitude regions showing a negative trend (decrease in crop yields) overall. The uncertainty at mid-latitude regions is likely due to the more dynamic climate of this area, and not indicative of contradictory data, or improper models.

2.3. Effects of Climate Change on Global Food Production Under SRES Emissions and Socio-economic Scenarios

The HadCM3 is a global climate model used to predict climate change impacts. It was developed under guidance of the Intergovernmental Panel on Climate Change Special Report on Emission Scenarios (SRES). The modeling system is able to consider crop yields, production and socio-economic, and climate variables effecting risk of hunger. Crop production simulations are translated into four computational methods (A1F1, A2, B1, and B2). This method of computation further considers global aggregation of crops to pinpoint sources of deficiency based on the considered variables. Each of the computational methods show variables: A1F1 shows the greatest decline overall by the 2080's, while A2 a-c highlights the largest disparity between developed vs non-developed countries, for example. When the models are considered in the Basic Linked System BLS, overall the world should be able to sustain itself, despite decline in global production. However it is important to note the continued sustainment will

only be achieved through a careful balance of understanding population dynamics in developed vs non-developed countries and allocation of resources to compensate for regional loss of production.

2.4. Climate Change and the Middle Atmosphere. Part I: The Doubled CO_2 Climate

An examination of the effect on increased CO_2 and climate changes was completed using the GISS global climate/middle atmosphere model. The simulation aims to determine the effect of doubled CO_2 on the stratosphere and troposphere, while sea surface temperatures are increased according to the predictive modeling values using an independent modeling system. Additionally, the middle atmosphere was analyzed to determine transient effects by allowing it to only react radioactively. The modeling shows doubling CO_2 affects the troposphere and stratosphere temperatures differently. As CO_2 rises, the troposphere temperatures rise, and the astrosphere cools. This is due to the height of CO_2 in the atmosphere and blocking radiative energy from the surface from reaching the stratosphere. This difference in temperatures reduces the static stability potential on the atmosphere. This results in increased eddy energy generating increased propagation of waves. As wave propagation increased (equatorial to polar) more heat is transferred to the poles (increase in circulation). This results in warming of higher latitudes.

2.5. High-Throughput Synthesis of Zeolitic Imidazaloate Frameworks and Applications to CO_2 Capture

Zeolites may be a promising solid support for CO_2 capture. This paper examined a high-throughput protocol to synthesize imidazaloate frameworks. The synthesis resulted in 25 different crystal networks of either cobalt(II)/ zinc(II) and imidazaloate/imidazaloate-type likers.

This resulted in new compositions and structures and new topologies never seen in zeolitic compounds. Three members of this group (ZIF-68, ZIF-69, and ZIF-70) are good candidates due to their high thermal stabilities (up to 390°C), chemical stability in both organic and aqueous solutions (under reflux) and high overall porosity (BET surface areas up 1970 m2/g), and high selectivity for CO_2. The listed values of CO_2 efficiency are measured in liters (83 $L_{CO}^2/L_{ZIF\text{-}69}$) at ambient temperature and pressure.

2.6. A Comparison of Gas Adsorption on Metal Organic Frameworks Using a Sticking Factor Concept

Metal Organic Frameworks are an option for solid support for CO_2 capture. They have been considered previously as hydrogen storage medium, and a correlation has been described relating MOF's physical parameters and hydrogen sticking efficiencies [14] .This was further investigated to determine if the sticking efficiency coefficient held true for other gasses (e.g. methane, CO_2). Different MOF's were utilized in this experiment, and were tested at both high pressure and low pressure (1 atm). It was shown that the sticking efficiency coefficient as it is currently modeled is not the best predictor of CO_2 adsorption, however good measurements of CO_2 efficiency at ambient pressure were recorded and the highest CO_2 capacity MOF (weight %) is Mg-MOF-74.

2.7. Sponges with Covalently Tethered Amines for High-efficiency Carbon Capture

A novel approach to carbon capture using in-situ covalently tethered polyethylimine (PEI) to mesoporous silica foam was demonstrated [19]. This study attempts to solve two problems in amine functionalized silicas for carbon capture, amine loading and blocking, and overall CO_2

capture efficiency. By covalently tethering PEI to a silica sponge, they were able to demonstrate high amine loading (>15 mmol N g^{-1}) and high CO_2 capacity (> 8mmol g -1). Furthermore, the amine functionalized silica shows high recyclability, and relatively low regeneration cost compared to other classes of solid supports (e.g. zeolites, activated carbons MOFs). Their results are consistent with other published literature, and may offer a next step, in grafting and functionalization of solid silica supports for both carbon capture and possible drug delivery. Various other solid sorbent alternatives to the solution-based CO_2 absorption systems have been investigated to date, including amine-functionalized polymers, ionic liquids, solid-supported amines, amine-grafted porous carbon [16, 17, 20, 22, 24, 30].However, often such systems present low absorptivity (~ 2 mmol CO_2/g absorbent) and sophisticated synthetic methodologies, which would render them expensive in a practical application.

2.8. Facile Synthesis of Controllable Dendritic Mesoporous Silica

Dendritic mesoporous silicas were evaluated [27]. Overall, they exhibited high hydrothermal stability (morphology and pore structure remained during steam treatment at 700°C for 6 hours). However, the size controllable synthesis of dendritic MSNs by this methodology is not realized due to the intrinsic nature of this method, i.e. the nucleation and growth of dendritic MSNs is not sensitive to the modulation of reaction parameters such as temperature and volume ratio of water to ethanol. This highlights two important parameters to consider in choosing a size control agent to synthesize dendritic MSN's with uniform and tunable pore size of a specified morphology. The size control agent must not interfere with the

self-assembly mechanism between surfactants and silicates. Also, it must not change the reaction conditions such as the pH of the reaction medium.

Further investigation of silica nanoparticles, nano-zeolites, metal-organic frameworks, and other inorganic-organic hybrids, proved that ionic liquid and nonionic block copolymer can act as good size-controllable agents for the synthesis of dendritic MSNs with a systematic investigation of the type and amount of methyl-imidazolium ILs and concentration of Pluronic on the particle size of dendritic MSNs. SEM images reveal that the addition of certain reactants that fit that meet the two qualifications above, directly affect the morphology (distance between "wrinkles"). The addition of different co-solvents such as n-butanol and 2-propanol in the reaction media alters the morphology and particle size of dendritic MSNs. Increasing distance between wrinkles, likely resulted in a decrease in surface area. Furthermore, it was noticed that an increase of conductivity (increased ionic potential) of reaction medium positively correlates to the growth rate of MSNs nanoparticles, facilitating the formation of MSNs with larger size.

This difference of surface area between MCM-41 and dendritic MSNs further evidence suggests that the dendritic MSN was formed by the weak self-assembling interaction between silica and ionic surfactant, instead of classical synergetic self-assembling formation mechanism.

2.9. Facile Large-Scale Synthesis of Monodisperse Mesoporous Silica Nanospheres with Tunable Pore Structure

Despite the work supporting morphology directed MSN synthesis, synthesizing a controllable pore network with monodispersed sizes under 200 nm has been challenging. Control of pore size and structure is poor without the use of additives to the traditional silica

nanoparticle synthesis. It has been shown that radial oriented mesochannels are possible using micro emulsion media which produces conical pore shapes.

Chemical stability, consistent pore structure, easy large-scale purification, and recovery from colloidal solutions are required for any industrial application of MSNs. Soft-templating synthesis of MSNs is the best and easiest method because there is little aggregation, involving a well-defined pore structure, uniform morphologies, and particle size control. Under similar synthesis conditions, the substitution of Br- ions led to monodispersed quasi-spherical MSNs with spherical pores [29].

The structural uniformity of the MSNs allowed the most consistent measurement of pore size from both TEM and N2 physiosorption isotherms and confirmed the pore templating mechanism by single spherical CTAB micelles. High surfactant and silanolate densities result in stronger templating conditions. This produces MSN's with a highly organized one dimensional structure (worm-like organized pore channels). High thermal stability is recognized (700°C) due to the thicker pore walls.

While stellate channel morphology appears to be kinetically driven through nucleation around aggregated micelles, it is more likely that self-assembly of partially silicate micelles drives growth. This is for solutions in which the surfactant concentration is below the surfactant critical micelle concentration. This supports that a three-step formation mechanism is appropriate for describing the synthesis of all three types of MSN morphologies, in which self-assembly takes place between polymerizing silicate oligomers and individual surfactant micelles.

2.10. Large-Pore Ultrasmall Mesoporous Organosillica Nanoparticles: Micelle/Precursor Co-templating Assembly and Nuclear-Targeted Gene Delivery

MONs were produced as a means to increase the pore volumes of stellate shaped silica nanoparticles utilizing Bis[3-(triethoxysilyl)propyl]tetrasulfide (BTES) as a pore swelling agent [25]. MONS begin with similar reaction conditions (micellated surfactant in diH_2O), and use TEOS as the silica precursor. BTES is an amphiphilic molecule; the non-polar section folds and inserts itself into the non-polar region of the micelle, leaving the polar silica tails exposed. MONs exhibit large surface area (613.9 m^2/g) and extremely high pore volume (2.19 cm^3/g). Similar to other silica nanoparticle formulae, MONS have tunable pores by altering molar ratios of surfactants (TEA) and pore swelling agents (BTES). The aim of this research was to use MONS to act as vectors for larger bio macromolecules (nucleic acids). As such, the biocompatibility was tested and MONS show relatively high biocompatibility. Another factor in gene delivery is modifying the surface of a potential vector to target specific sites within the cell. MONs are able to be surface modified with amine groups for this purpose. While this research was focused on bioapplications for gene therapy, the ability to enlarge pores via pore swelling agents may be used for modifying silica platforms used in carbon capture.

2.11 Dendritic Silica Particles with Center-Radial Pore Channels: Promising Platforms for Catalysis and TEPA for Biomedical Applications

This study evaluates multiple dendritic silica particles, their characteristics, varying synthesis, and different applications [7]. Aside from the common sol-gel synthesis, several new syntheses have been developed (e.g. biphase stratification, micro-emulsion, ethyl ether emulsion, styrene

emulsion) and offer different morphologies and properties. Furthermore, more complex morphologies can be designed involving a core-shell and either fibrous or wrinkle type silica dendrimers. Each of these has applications in varying fields. The use of silica, again is desirable due to facile synthesis, bio-compatibility and in some cases large (kg) scale-up. The diversity of silica NP's and synthesis, show a needed shift in focus from development to research in new applications.

CHAPTER 3. MATERIALS AND EXPERIMENTAL DESIGN

3.1. MATERIALS

MSN: Hexadecyl-trimethyl-amonium bromide and tetraethyloxysilane were purchased from Sigma-Aldrich. Methanol was purchased from VWR International. Sodium Hydroxide was purchased from Sigma-Aldrich and prepared as a molar solution in nanopure water. Nanopure water was deionized to 18.2 MΩ ionic purity in a PURELAB Flex 3 (Elga) system and used for the synthesis of MSN materials.

PSP series: Triethanolamine was purchased from VWR International. Hexadecyltrimethylammonium p-toluenesulfonate was purchased from Sigma-Aldrich. Methanol was purchased from VWR International. Nanopure water was deionized to to 18.2 MΩ ionic purity in a PURELAB Flex 3 (Elga) system and used for the synthesis of PSP materials.

MONs: 1-Hexadecyl)trimethylammonium chloride was purchased from Alfa Aesar. Bis[3-(triethoxysilyl)propyl]tetrasulide was purchased from Sigma-Aldrich. Nanopure water was deionized to to 18.2 MΩ ionic purity in a PURELAB Flex 3 (Elga) system and used for the synthesis of MONS materials.

Functionalized PSP: Tetraethylenepentamine and polyethylenimine were purchased from Sigma Aldrich. (3-Aminopropyl)triethoxysilane was purchased from Alfa Aesar. Green Fluorescent Protein was produced within the laboratory using protein expression and purification protocols. Trypsin was purchased from Thermo Fisher. Doxorubicin was purchased from

Sigma-Aldrich. Nanopure water was deionized to 18.2 MΩ ionic purity in a PURELAB Flex 3 (Elga) system and used for the synthesis of functionalized PSPs.

3.2. CHARACTERIZATION EQUIPMENT

A Quantachrome NOVA 4200e Surface Area & Pore Analyzer was used to perform nitrogen isotherm physiosorption measurements. Isotherm data was collected at 77K for porosity characterization. The isotherm data was fit using standard models reported in literature and surface area, calmative pore volume, average pore size, pore size distribution, were calculated. Multi-point BET (>0.05 - >0.30 P/Po) was used for surface area measurements. The NLDFT and BJH models were used to quantify cumulative pore volume and pore size distribution. For the BJH model, the adsorption branch was used to perform calculations. Average pore size was calculated using Quantachrome's propriety software NOVAWin, using the isotherm data and BET data in the following model: (Nova 11.0 Rev-x pg 79) where S is the BET surface area, and V-liq is the volume of nitrogen adsorbed (V-ads). V-liq is calculated from the isotherm results and is defined as the volume of liquid nitrogen and is calculated from V-ads using the following model: (Nova 11.0 Rev-x pg 79) where Pa and T are ambient pressure and temperature and Vm is the molar volume of the liquid adsorbate: 34.7 cm^3/mol is the value used by Quantachrome for this calculation.

A PerkinElmer Thermogravimetric Differential Thermal Analyzer (TG/DTA) was used to perform decomposition and carbon capture efficiency. The carbon capture efficiency data was collected from the TG/DTA, plotted in Microsoft Excel (year) and calculated in mmol/g.

A Shimadzu IR Prestige 21 Fourier Transformation Infra-Red spectrophotometer (FTIR) was used to evaluate the presence of functional groups in functionalized nanoparticles. Spectrum data was collected, plotted in Microsoft Excel and analyzed.

3.3. METHODS

MSN-41 was used as a baseline for which to compare other morphologies due since its characteristics (e.g. surface area, pore size, pore uniformity, monodispersed size, etc.) are well known. In a 1,000 ml round bottom flask, 2 g of CTAB and 7.0 ml of NaOH were added to 480 ml of nanopure H_2O and stirred at 80 C for about 1 hr (until all CTAB was dissolved). 10.0 ml of TEOS was then quickly added and the solution allowed to stir for another 2 hours.

The solution was collected and washed with 1 volume of nanopure water and 2 volumes of MeOH under vacuum filtration. The dried solution was then placed in a vacuum oven overnight at 50°C. The as synthesized MSN-41 was collected, characterized, and the template was removed by either calcination or acid wash. The calcinated material was heated to 550°C using the listed ramp plot.

Next, 2 g of the AS material was collected and placed into a 250 ml round bottom flask with 160 ml MeOH and 9 ml of 37.4% HCL. The solution was stirred for 24 hr, collected, and washed with 2 volumes of methanol under vacuum material. The dried material was placed into a vacuum over overnight at 50°C and collected the following day. Both the calcinated material and acid washed material were characterized and compared against each other and the AS material.

Porous Silica Platform (PSP) is a modification of the above synthesis and produces a stellate shaped silica nanoparticle with a hierarchical pore structure. In a 250 ml round bottom flask 0.4 g of TEA and 1.920 g of CTATos were added to 100 ml of nanopure H_2O and allowed to stir at 80°C for about 1 hour (until CTAT is dissolved). 14.58 g of TEOS was quickly added and the solution allowed to stir for an additional 2 hr.

The solution was collected, filtered, dried, characterized, and processed (calcination/acid wash), with the procedures listed above. The calcinated and acid wash versions were also characterized using the same method listed previously for MSN-41AW and MSN-41CAL.

In an attempt to increase carbon capture efficiency, a pore swelling agent was used to synthesize Mesoporous Organosillica nanoparticles (MONS) using the method described in the literature. In a 100 ml round bottom flask 1.6f of TEA and 4 g CTACl was added to 40 ml of nanopure water and stirred for approximately 1 hr (until CTACl was dissolved). A solution of 2.143 g or TEOS and 2.407 ml of BTES was prepared, added drop wisely to the solution and allowed to stir for an additional 4 hr. The material was collected was collected, filtered, dried, characterized, and processed as outlined above.

MSN-41 and PSP (AS, AW, and CAL) were functionalized with TEPA as the functional amine for carbon capture. In a 20 ml reaction vial, 0.5 g of silica material was added to 7 ml of EtOH and sonicated at 42 KHz for 15-20 mins. A TEPA stock was made by adding 0.5 g of TEPA to 5 ml of EtOH and vortexed. 3.75 ml of TEPA stock was added to the sonicated material and stirred for 4-6 hrs at 60°C. The functionalized material was collected and dried in a vacuum oven overnight at 50°C.

MSN-41 and PSP (AS,AW, and CAL) were functionalized with PEI as the functional amine for carbon capture and prepared per the synthesis outlined for TEPA above.

MSN-41 and PSP (AW and CAL) were loaded with GFP for fluorescent microscopy. GFP was produced using a plasmid encoding for GFP protein , and E. Coli BL21. The bacteria were cultured on kanamycin agar plates and single colonies were selected. The single colonies were cultured in a 5 ml culture tube for 12 hr, and then transferred to 250 ml of Lauria Broth and grown to an optical density of 600 OD. The BL21 were then induced with 100 uL of IPTG to express the GFP and grown overnight. The cultures were collected and centrifuged. The supernatant was poured off and the pellet was resuspended in 1 ml of OTG. The lysed culture was centrifuged and the supernatant was collected and purified. The purified GFP was then loaded into the nanoparticle of interest. The 0.5 g of nanoparticle material was sonicated in 5 ml of PBS. The 1 ml of purified GFP was added to the sonicated solution and allowed to mix overnight.

CHAPTER 4. RESEARCH FINDINGS AND DISCUSSION

4.1. Amine Content in Stellate MSN

The actual amine content was evaluated by thermogravimetric analysis (TGA). In a typical experiment, the amount of weight loss versus temperature (from 273 to 1073 K) was measured for pre-weighed quantities of TEPA-loaded stellate MSN. The data enable the evaluation of both stability of the resulting TEPA-stellate MSN and the amount of amine coverage. **(Table 1**).

Table 1. TEPA Loading in Stellate.

TEPA-stellate MSN	Amine (TEPA) loading (mmol/g sorbent) obtained by TGA
W03	2.23
W06	3.39
W075	4.56
W1	6.94

In addition, FTIR was used to cofirm the presence of TEPA once loaded. Each TEPA concentration was measured as well as the unloaded Stellate MSN (**Figure 8).** The structure of the silica nanospheres, studied by transmission electron microscopy (TEM), illustrates both the large pores and the full pore accessibility upon TEPA impregnation **(Figure 9a and 9b).** This is further confirmed by porosity data indicating that at any TEPA loading, access to pores is not impaired. Nitrogen adsorption–desorption isotherms of the stellate MSN and TEPA-stellate MSN were obtained on a Nova 4200e surface area and porosity analyzer (Quantachrome, Boynton Beach, FL) in the relative pressure P/P0 range of 0–0.95 at 77 K. TEPA- loaded stellate

MSN was degassed at 110°C for 3 hr under high vacuum in order to account only for TEPA that is stably impregnated into stellate MSN.

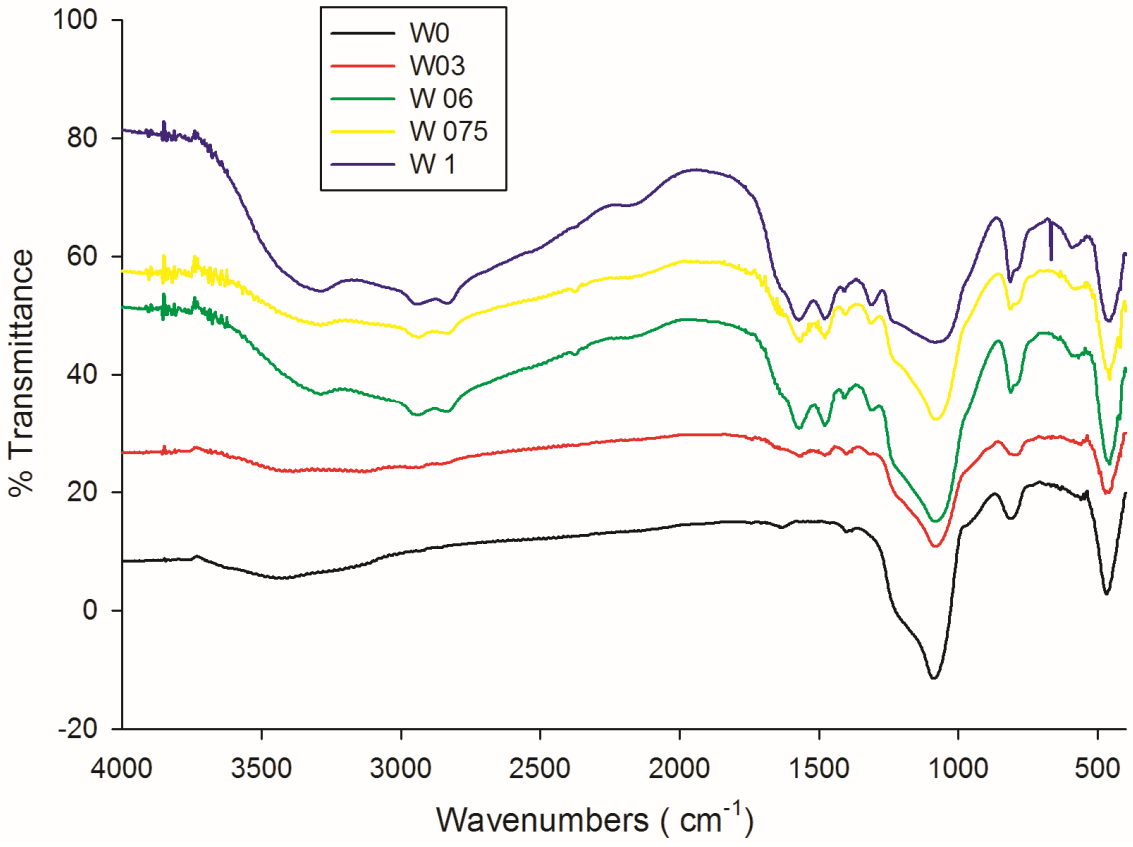

Figure 8. FTIR spectra of the TEPA loaded Stellate MSN sorbent samples were obtained using the FTIR spectrometer. For W0 an Si-O_2 stretch is present (1060-1080 cm^{-1}). In the other samples, a C-H stretch (2800-3000 cm^{-1}), N-H stretch (3300-3500 cm^{-1}), and C-N stretch (1180-1360 cm^{-1}), are present in increasing intensities confirming successful TEPA loading.

The total pore volume was calculated as the adsorbed volume of liquid nitrogen at the relative pressure of P/P0 0.95. Specific surface areas were calculated using the Brunauer–

Emmett–Teller (BET). The isotherms (Figure 10) show full pore accessibility upon TEPA loading (no hysteresis) except for the W1 material.The W1 isotherm suggests that the loading

exceeded the surface coverage and points to W075 as an optimal loading, where the access to pores is not impacted (same adsorption–desorption path). The BET-determined surface areas of the stellate MSNs before and after TEPA loading are showed in Table 2. The FT-IR data do not show significant difference among the TEPA-loaded materials, suggesting that amine coverage is present in all materials, however, it show the presence of amine in comparison with the non-functionalized material W0.

The porosity data indicate that although the reported work on stellate silica refers to this material as mesoporous, the type II isotherm is a clear indicator of macroporosity, which is consistent with the large hierarchical pores of the stellate materials [22].

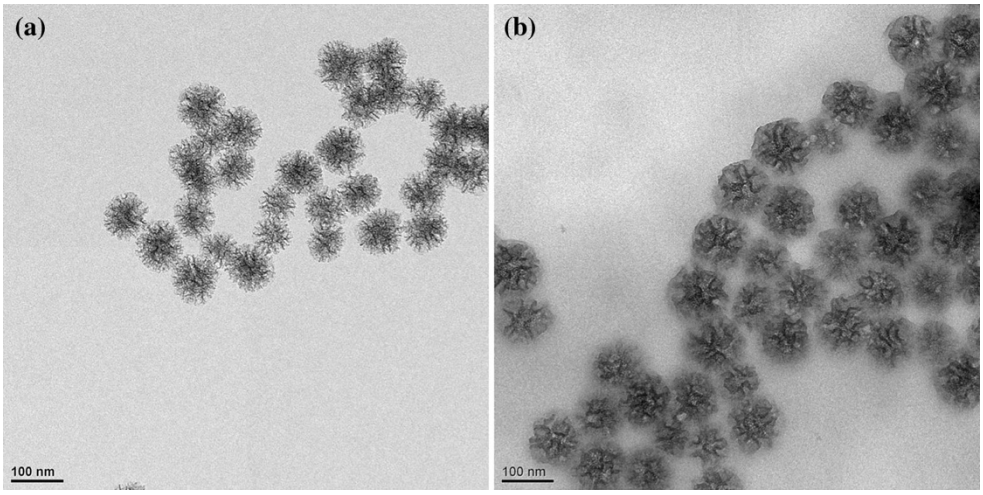

Figure 9. Stellate MSN before (micrograph a) and **(b)** after TEPA impregnation (micrograph b) with 6.9 mmol TEPA/gram of stellate MSN.

We are therefore referring to the stellate silica nanospheres as macroporous. The macroporosity of the materials is maintained upon TEPA loading, as illustrated in **Figure 10.**

The amine coverage could be estimated by compiling the data from the TGA and BET, if assuming a uniform coverage of the surface**.** The surface of the pores is decreasing with increased TEPA loading, an expected result for any functionalization method.

Table 2. BET surface area of stellate MSN and TEPA-loaded MSN.

Material ID	**BET surface area (m^2/g)**	**Amine content by TGA (mmol/g)**	**Amine coverage ($mmol/m^2$)**
W0	508.6	0.00	0.00
W03	220.4	2.23	10.12
W06	195.4	3.93	20.11
W075	193.5	4.56	23.58
W1	139.3	6.94	49.83

4.2. CO2 Capture Experiments

The TEPA-stellate MSN materials were subjected to carbon dioxide capture experiments designed to determine absorptivity of pure CO_2 in the amine- functionalized materials. The CO_2 capture was measured using thermogravimetric (TGA) analysis by monitoring the weight gain of the material over a predetermined period of time. The measurements were performed at temperatures in the range of flue gas temperature, which typically is cooled to 30–80 °C in actual power plants. The performance of our materials at both low and elevated temperatures **(Figure 11)** indicates their excellent potential for CO_2 capture.

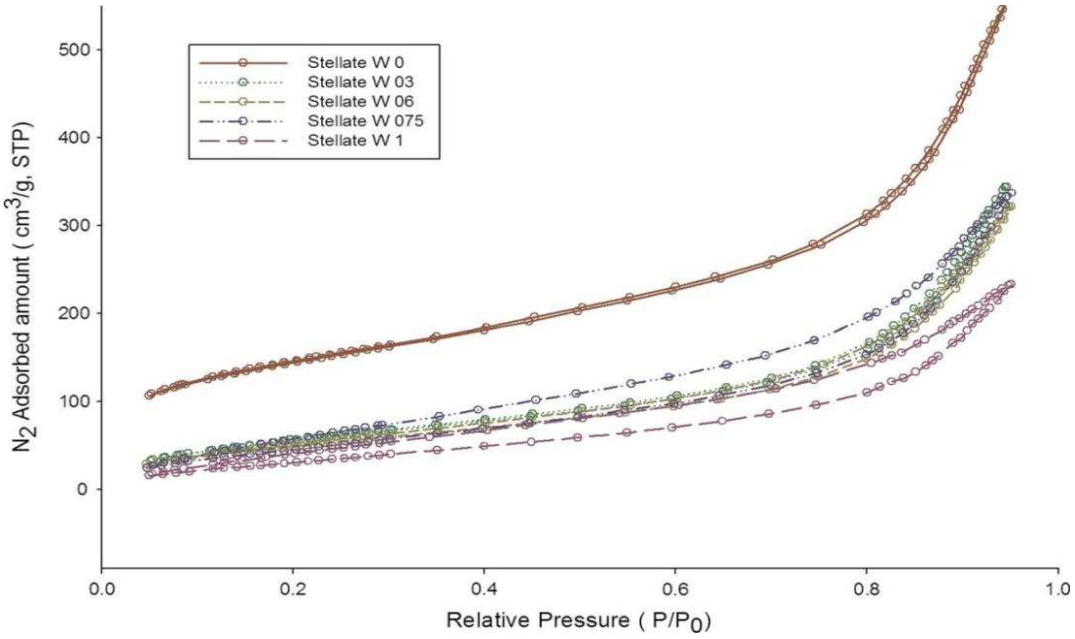

Figure 10. Nitrogen adsorption and desorption isotherms for stellate MSN before (W = 0) and after TEPA loading (at each loading amount).

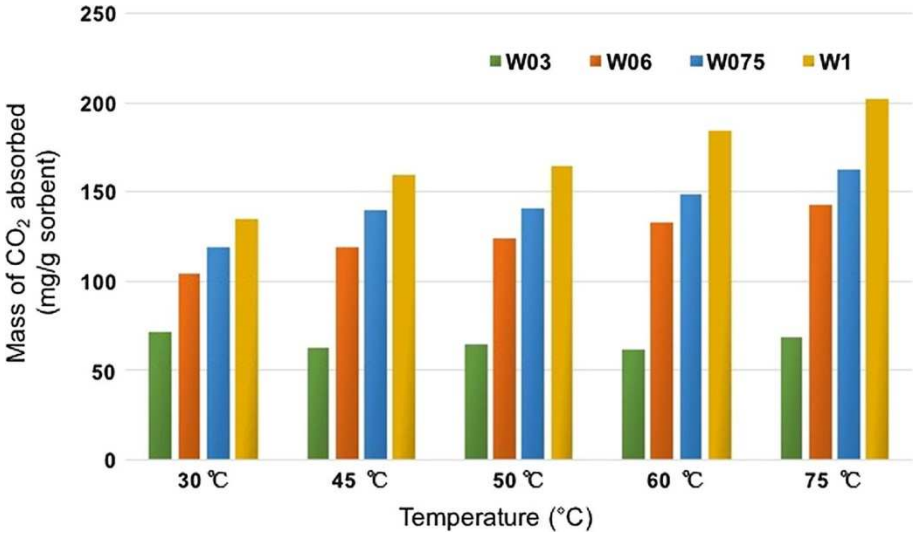

Figure 11. CO_2 absorption in TEPA-stellate MSN (mg CO_2/ g absorbent).

To understand how the materials compare in respect to amine coverage and amine groups accessibility, the amine efficiency was evaluated for the four materials treated with TEPA **(Figure 12).** The nitrogen efficiency calculations accounted for 5 mmol nitrogen/each mmol amine. The data suggest that the amine accessibility reaches a plateau at 4.56 mmol amine/gram TEPA- stellate MSN (material W075 in **Table 1**). This is in agreement with the porosity data **(Figure 10**) showing hysteresis in the W1

material, which is not present for the other three tested materials. The typical flue gas composition involves a mini- mum of 70 % N_2 and in contrast to current industrial solution scrubbing; the solid sorbents could pose the challenge of N_2 absorption. To understand the CO_2 selectivity of the materials in respect to N_2, the top performing materials in our study have been subjected to N_2 and CO_2, respectively, at room temperature 25 and 0°C. The experiments validate the regeneration capacity of our platform showing an almost imperceptible decrease in sample weight at each step, which could be also related to sample handling due to gas flow and very low density of the stellate MSN (data presented for W1 material in **Figure14**).

Figure 13 shows the absorption curves for the stellate MSN W075. The experiments were conducted in a Nova 4200e surface area and porosity analyzer (Quantachrome, Boynton Beach, FL).

To achieve market competitiveness in implementation of GHG-mitigation technologies for CO_2 capture, an inexpensive platform, with high reusability, would be required. We evaluated the recyclability of the material for the stellate MSN W1, provided that it shows the highest absorbance capacity. **Figure 14** shows the absorptive capacity of W1 material tested in nine consecutive cycles, showing high robustness over a 30–80°C temperature range.

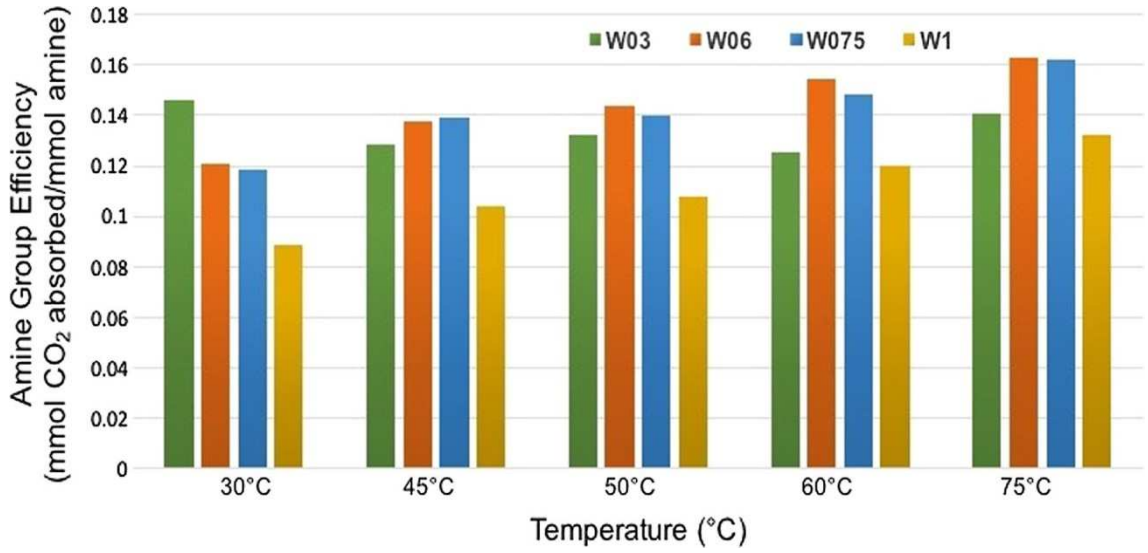

Figure 12. Amine efficiency in TEPA-stellate MSN

T

he

experim

ents validate the regeneration capacity of our platform showing some decrease in sample weight at each step, which could be also related to sample handling given the presence of the gas flow and very low density of the stellate MSN (data presented for W1 material in **Figure 14**). Material loss observed **(Figure 14)** upon nine cycles was evaluated at 14 % suggesting a TEPA loss, given that the CO_2 absorbing performance, calculated per amount of available material, is maintained at 86%.

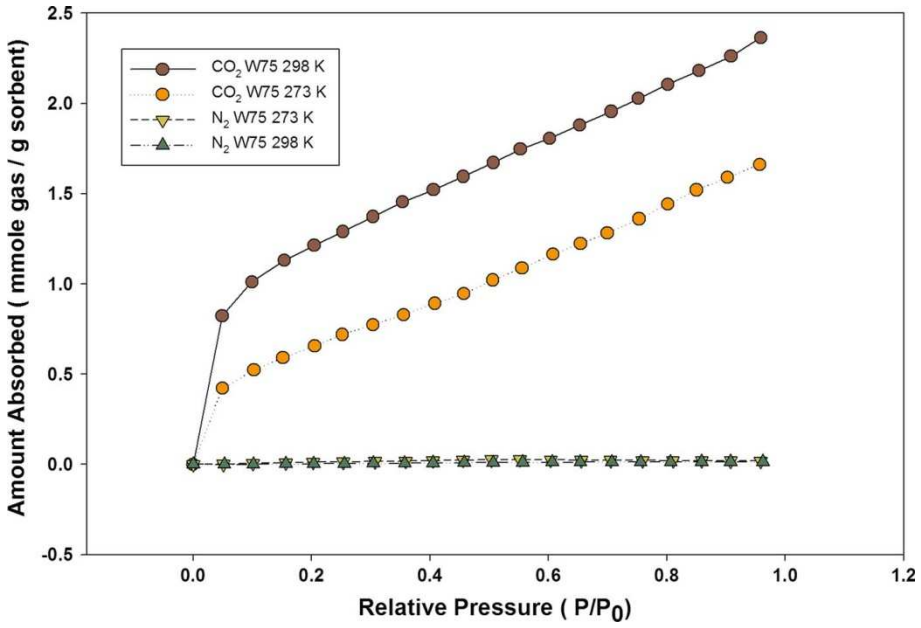

Figure 13. CO_2 versus N_2 sorption selectivity.

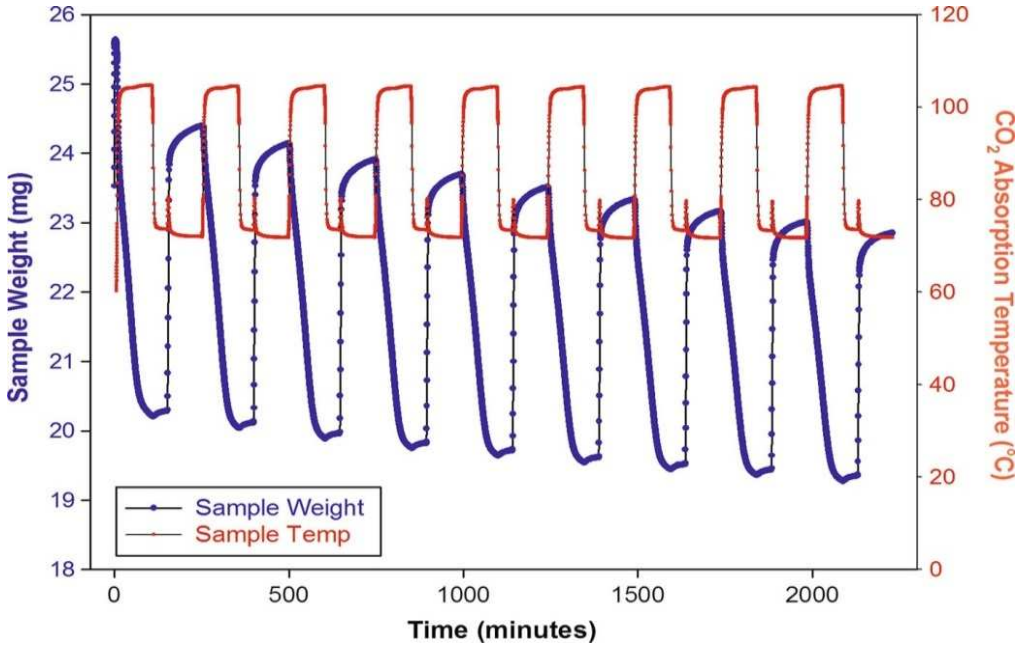

Figure 14. TEPA-stellate MSN W1 stability upon absorption/ desorption.

CHAPTER 5. CONCLUSIONS AND FUTURE RECOMMENDATIONS

Surface functionalization with amines by non-covalent interactions (impregnation) or covalent interactions (via grafting or co-condensation) could convert silica nanospheres into an advanced functional material with (CO_2) capture capacity. We have utilized stellate MSN as a scaffold to anchor a pentamine, TEPA, via non-covalent interaction, to the silica pore wall. The interior surface of the materials after TEPA impregnation ranges from 139.28 to 220.36 m^2/g for TEPA-stellate MSN which inversely correlates with the amount of amine loading **(Table 1**). The experimental work demonstrated that the stellate MSN could uptake up to 6.94 mmol of TEPA per gram which points to a theoretical capacity of CO_2 absorption of at least double (13.92 mmol CO_2), assuming that the terminal TEPA group is used to non-covalently attach to the silica pore and the rest of the four amines are capturing at least two molecules of CO_2 **(Figure 1**). The overall amine efficiency is therefore low; suggesting that further optimization of this platform could lead to superior capture. In addition, in comparison with the published data on optimized stellate MSN scaffold, reporting 689 m^2/g, our surface area of W0 (non-functionalized silica scaffold) was measured as 508.6 m^2/g, and therefore, further optimization could improve significantly the CO_2 capture.

The experimental work is proving the concept of CO_2 capture for TEPA-functionalized stellate MSN using pure CO_2. Comparing the sorption isotherms for CO_2 at 273 and 298 K, the material shows excellent selectivity for CO_2 given that flue gas contains [70% N_2. We have also

demonstrated that the material is highly reusable and thus, provides a feasible alternative to amine solution scrubbing.

The high CO_2 capture performance along with stability and recyclability of the amine-functionalized TEPA-stellate MSN materials indicate their strong potential for further evaluation in emerging CO_2 capture technologies. In the series of materials tested, the highest absorption capacity reached over 100 mg CO_2/gram of W1, a number that exceeds currently reported results in silica–amine platforms. Based on the low amine usage efficiency, improvements in silica scaffold, and subsequent increase in the surface area of un-treated silica are potential paths to further improve the CO_2 capture capability of the stellate MSNs.

REFERENCES

[1] Bae, S.; Ma, K.; Kim, T. H.; Lee, E. S.; Oh, K. T.; Park, E.-S.; Lee, K. C.; Youn, Y. S., Doxorubicin-loaded human serum albumin nanoparticles surface-modified with TNF-related apoptosis-inducing ligand and transferrin for targeting multiple tumor types. *Biomaterials* **2012,** *33* (5), 1536-1546.

[2] Berger, E.; Hahn, M. W.; PrzybillaThomas, B.; Winter, B.; Spiecker, E.; Jentys, A.; Lercher, J. A., Impact of solvents and surfactants on the self-assembly of nanostructured amine functionalized silica spheres for CO2 capture. *Journal of Energy Chemistry* **2016,** *25* (2), 327.

[3] Builes, S.; López-Aranguren, P.; Fraile, J.; Vega, L. F.; Domingo, C., Analysis of CO2 Adsorption in Amine-Functionalized Porous Silicas by Molecular Simulations. *Energy & Fuels* **2015,** *29* (6), 3855-3862.

[4] Crowley, T. J., Causes of climate change over the past 1000 years. *Science* **2000,** *289* (5477), 270-7.

[5] Danon, A.; Stair, P. C.; Weitz, E., FTIR Study of CO2 Adsorption on Amine-Grafted SBA-15: Elucidation of Adsorbed Species. *The Journal of Physical Chemistry C* **2011,** *115* (23), 11540-11549.

[6] Didas, S. A.; Choi, S.; Chaikittisilp, W.; Jones, C. W., Amine–Oxide Hybrid Materials for CO2 Capture from Ambient Air. *Accounts of Chemical Research* **2015,** *48* (10), 2680-2687.

[7] Du, X.; Qiao, S. Z., Dendritic Silica Particles with Center-Radial Pore Channels: Promising Platforms for Catalysis and Biomedical Applications. *Small* **2015,** *11* (4), 392-413.

[8] Figueroa, J. D.; Fout, T.; Plasynski, S.; McIlvried, H.; Srivastava, R. D., Advances in CO_2 capture technology—The U.S. Department of Energy's Carbon Sequestration Program. *International Journal of Greenhouse Gas Control* **2008,** *2* (1), 9-20.

[9] Hahn, M. W.; Jelic, J.; Berger, E.; Reuter, K.; Jentys, A.; Lercher, J. A., Role of Amine Functionality for CO2 Chemisorption on Silica. *The Journal of Physical Chemistry B* **2016,** *120* (8), 1988-1995.

[10] Han, B.; Zhou, C.; Wu, J.; Tempel, D. J.; Cheng, H., Understanding CO2 Capture Mechanisms in Aqueous Monoethanolamine via First Principles Simulations. *The Journal of Physical Chemistry Letters* **2011,** *2* (6), 522-526.

[11] Harlick, P. J. E.; Sayari, A., Applications of Pore-Expanded Mesoporous Silica. 5. Triamine Grafted Material with Exceptional CO2 Dynamic and Equilibrium Adsorption Performance. *Industrial & Engineering Chemistry Research* **2006,** *46* (2), 446-458.

[12] Haszeldine, R. S., Carbon Capture and Storage: How Green Can Black Be? *Science* **2009,** *325* (5948), 1647-1652.

[13] Huang, Y.; Luo, Y.; Zheng, W.; Chen, T., Rational Design of Cancer-Targeted BSA Protein Nanoparticles as Radiosensitizer to Overcome Cancer Radioresistance. *ACS Applied Materials & Interfaces* **2014,** *6* (21), 19217-19228.

[14] Iriowen, E.; Goudy, A. A Comparison of Gas Adsorption on Metalorganic Frameworks Using a Sticking Factor Concept. International Journal of Advanced Research 2016, 4, 362-379.

[15] Li, K.-M.; Jiang, J.-G.; Tian, S.-C.; Chen, X.-J.; Yan, F., Influence of Silica Types on Synthesis and Performance of Amine–Silica Hybrid Materials Used for CO2 Capture. *The Journal of Physical Chemistry C* **2014,** *118* (5), 2454-2462.

[16] Liu, F.-Q.; Wang, L.; Huang, Z.-G.; Li, C.-Q.; Li, W.; Li, R.-X.; Li, W.-H., Amine-Tethered Adsorbents Based on Three-Dimensional Macroporous Silica for CO2 Capture from Simulated Flue Gas and Air. *ACS Applied Materials & Interfaces* **2014,** *6* (6), 4371-4381.

[17] Luo, X. Y.; Ding, F.; Lin, W. J.; Qi, Y. Q.; Li, H. R.; Wang, C. M., Efficient and Energy-Saving CO2 Capture through the Entropic Effect Induced by the Intermolecular Hydrogen Bonding in Anion-Functionalized Ionic Liquids. *J Phys Chem Lett* **2014,** *5* (2), 381-6.

[18] Radu, D. R.; Pizzi, N. A.; Lai, C.-Y. Functionalized stellate macroporous silica nanospheres for CO2 mitigation. *Journal of Materials Science* **2016**, 1-9.

[19] Qi, G.; Fu, L.; Giannelis, E. P., Sponges with covalently tethered amines for high-efficiency carbon capture. *Nature Communications* **2014,** *5*, 5796.

[20] Shi, Y.-Q.; Zhu, J.; Liu, X.-Q.; Geng, J.-C.; Sun, L.-B., Molecular Template-Directed Synthesis of Microporous Polymer Networks for Highly Selective CO2 Capture. *ACS Applied Materials & Interfaces* **2014,** *6* (22), 20340-20349.

[21] Sun, T.; Zhang, Y. S.; Pang, B.; Hyun, D. C.; Yang, M.; Xia, Y., Engineered Nanoparticles for Drug Delivery in Cancer Therapy. *Angewandte Chemie International Edition* **2014,** *53* (46), 12320-12364.

[22] Sun, L.-B.; Li, A.-G.; Liu, X.-D.; Liu, X.-Q.; Feng, D.; Lu, W.; Yuan, D.; Zhou, H.-C., Facile fabrication of cost-effective porous polymer networks for highly selective CO2 capture. *Journal of Materials Chemistry A* **2015,** *3* (7), 3252-3256.

[23] Thommes, M.; Kaneko, K.; Neimark, A. V.; Olivier, J. P.; Rodriguez-Reinoso, F.; Rouquerol, J.; Sing, K. S. W., Physisorption of gases, with special reference to the evaluation of surface area and pore size distribution (IUPAC Technical Report). *Pure and Applied Chemistry* **2015,** *87* (9-10).

[24] Wang, J.; Senkovska, I.; Oschatz, M.; Lohe, M. R.; Borchardt, L.; Heerwig, A.; Liu, Q.; Kaskel, S., Imine-Linked Polymer-Derived Nitrogen-Doped Microporous Carbons with Excellent CO2 Capture Properties. *ACS Applied Materials & Interfaces* **2013,** *5* (8), 3160-3167.

[25] Wu, M.; Meng, Q.; Chen, Y.; Du, Y.; Zhang, L.; Li, Y.; Zhang, L.; Shi, J., Large-Pore Ultrasmall Mesoporous Organosilica Nanoparticles: Micelle/Precursor Co-templating Assembly and Nuclear-Targeted Gene Delivery. *Advanced Materials* **2015,** *27* (2), 215-222.

[26] Xiong, L.; Du, X.; Shi, B.; Bi, J.; Kleitz, F.; Qiao, S. Z., Tunable stellate mesoporous silica nanoparticles for intracellular drug delivery. *Journal of Materials Chemistry B* **2015,** *3* (8), 1712-1721.

[27] Yu, Y.-J.; Xing, J.-L.; Pang, J.-L.; Jiang, S.-H.; Lam, K.-F.; Yang, T.-Q.; Xue, Q.-S.; Zhang, K.; Wu, P., Facile Synthesis of Size Controllable Dendritic Mesoporous Silica Nanoparticles. *ACS Applied Materials & Interfaces* **2014,** *6* (24), 22655-22665.

[28] Zhang, X.; Zheng, X.; Zhang, S.; Zhao, B.; Wu, W., AM-TEPA Impregnated Disordered Mesoporous Silica as CO2 Capture Adsorbent for Balanced Adsorption–Desorption Properties. *Industrial & Engineering Chemistry Research* **2012,** *51* (46), 15163-15169.

[29] Zhang, K.; Xu, L.-L.; Jiang, J.-G.; Calin, N.; Lam, K.-F.; Zhang, S.-J.; Wu, H.-H.; Wu, G.-D.; Albela, B.; Bonneviot, L.; Wu, P., Facile Large-Scale Synthesis of Monodisperse Mesoporous Silica Nanospheres with Tunable Pore Structure. *Journal of the American Chemical Society* **2013,** *135* (7), 2427-2430.

[30] Zhou, Y.; Liu, J.; Xiao, M.; Meng, Y.; Sun, L., Designing Supported Ionic Liquids (ILs) within Inorganic Nanosheets for CO2 Capture Applications. *ACS Applied Materials & Interfaces* **2016,** *8* (8), 5547-5555.